Chapter 4

Inversion of field data

In Chapter 3 I applied the method of CDR tomographic inversion to synthetic data. In this chapter I apply it to field data. Figure 4.1 shows the results of inverting the filtered, picked British Petroleum marine data shown in Figure 2.12 (page 33). The velocity model used in the inversion consisted of 500 grid boxes horizontally, and 150 grid boxes vertically. Each box was .01 km wide and .02 km tall. The damping parameters used in this inversion were $\lambda_x = .0312$ and $\lambda_z = .0052$ (the apparent high precision of these damping factors is an artifact caused by conversion from another system of units). Seven iterations were required for the inversion.

After experimentation I found that the inversion worked best when amplitude-based weighting (see section 3.3.2, page 45) was *not* used. Thus, all sets of reciprocal parameters were weighted equally. Experiments also showed that best results were obtained when a time shift of $-.05$ seconds was added to each picked value t. This time shift may have been necessitated by the shape of the wavelet in the original marine data. Figure 4.2 shows the justification for this time shift; it shows the amount of time shifting that would have to be applied to each set of reciprocal parameters from the water-bottom reflection in order to obtain a v_{CDR} equal to the water velocity (1.48 km/sec).

The velocity model in Figure 4.1 was used for the depth migration of the picked data (see section 3.5, page 53); Figure 4.3 shows the results of this migration. The length of each dip bar equals the residual value of x_{err} (defined in section 3.2.3, page 41). Thus, the longer dip bars represent picked parameters that do not fit the velocity model well—the opposite of what one would intuitively expect. Figure 4.3 does not show the results of depth migrating all the picked parameters; picks that have residual values of x_{err} greater

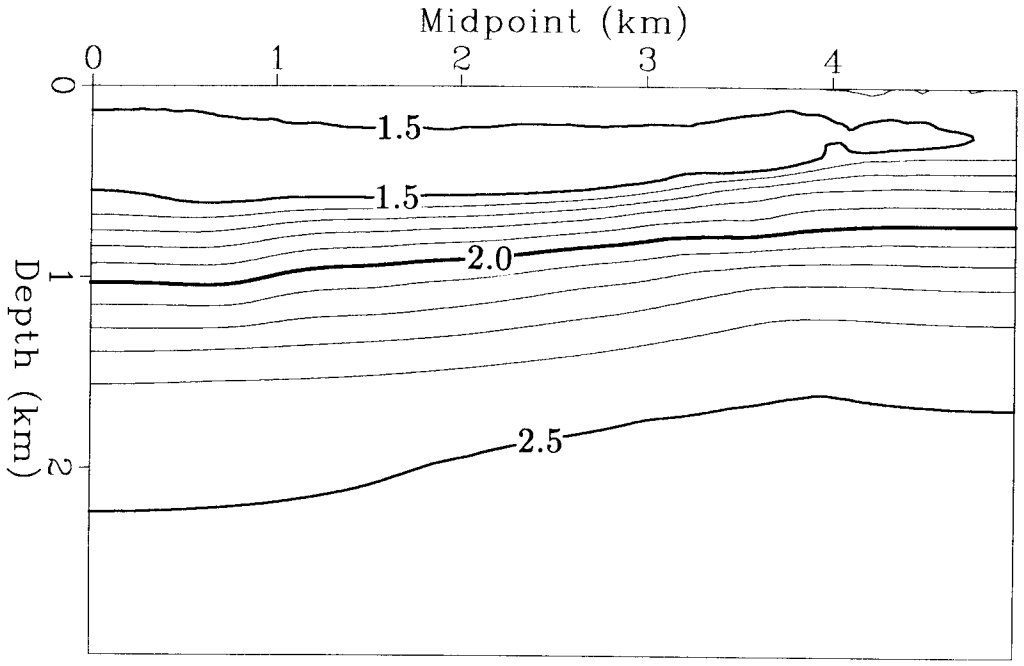

Figure 4.1: Results of inverting field data. This is the 7th iteration of the inversion process. The contour interval is .1 km/sec. The input data are shown in Figure 2.12 (page 33).

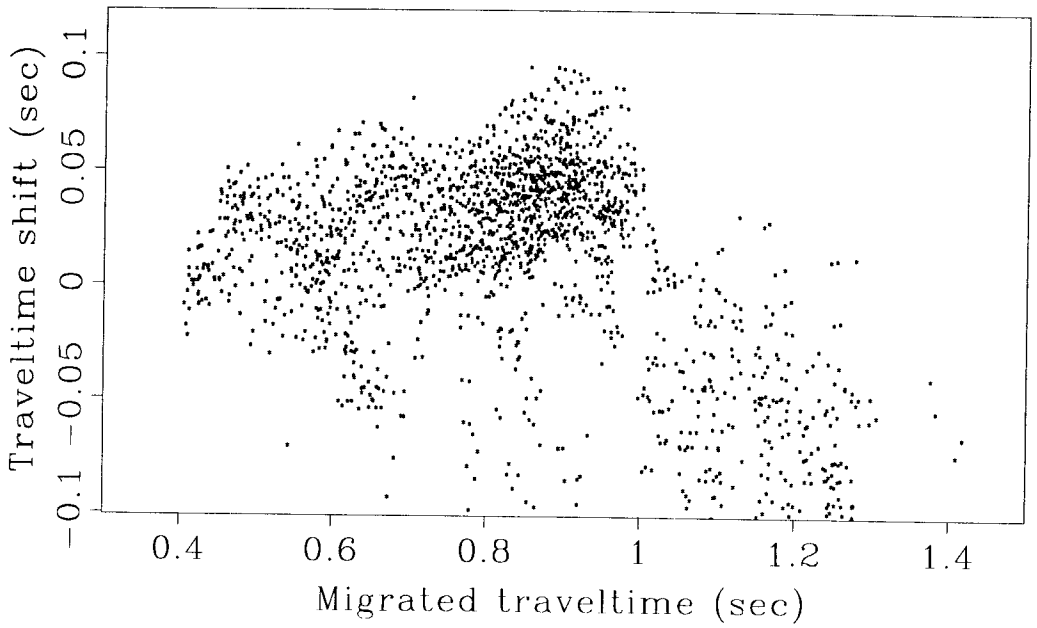

Figure 4.2: The need for a time shift. Each dot in this plot represents a set of picked parameters from the water-bottom reflection. The vertical axis shows the traveltime shift that is needed to bring v_{CDR} to water velocity (1.48 km/sec).

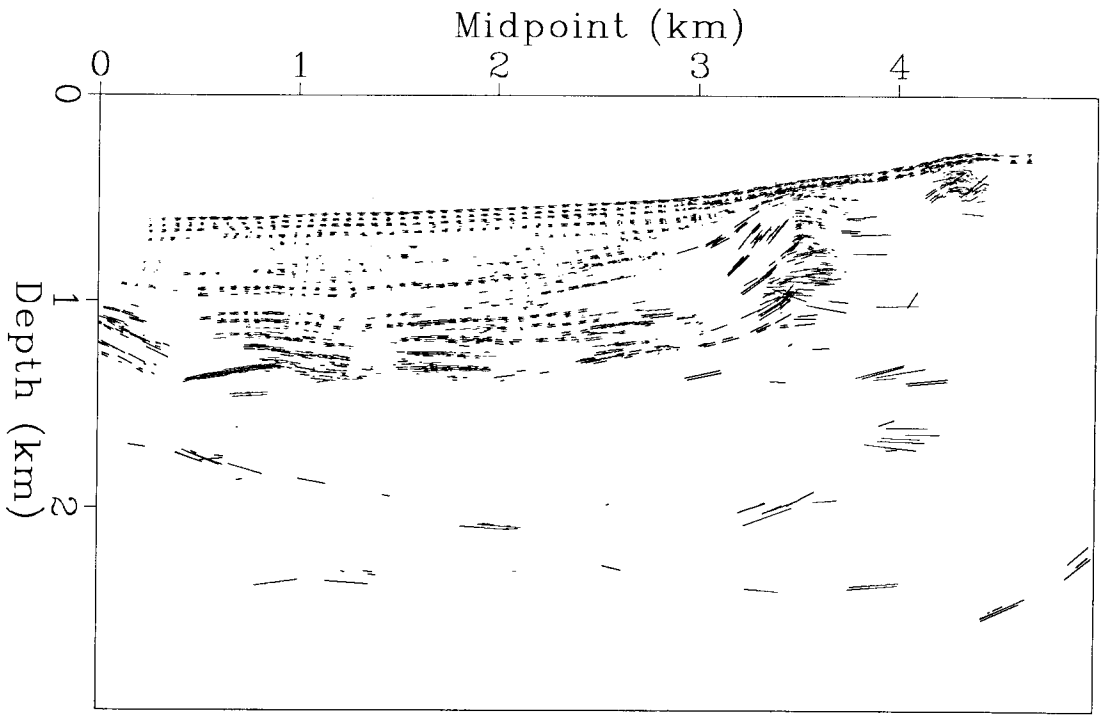

Figure 4.3: Depth migration using the inversion results. The velocity model in Figure 4.1 was used in a depth migration of the picked data. The length of each dip bar is equal to the residual value of x_{err}, so the longer dip bars represent poorer fits of the picked data to the velocity model.

than .13 km have been filtered out. Figure 4.4 shows a plot of midpoint versus residual x_{err}. The picked parameters whose x_{err} values fell outside the solid lines in Figure 4.4 (56 picks out of 3,244) were eliminated.

Figure 4.5a shows the same migrated dip bars as Figure 4.3, but with velocity contour lines superimposed. The contour interval in this figure is 1/4th that of Figure 4.1. Figure 4.5b shows the same information as Figure 4.5a, but with a 2-to-1 vertical exaggeration. It is encouraging that in many areas the contour lines follow the trend of the reflectors. By measuring the slight differences between the trend of the contour lines and the trend of the reflectors, it may be possible to draw some conclusions regarding the change in rock velocity with respect to compression.

In Figure 4.5 some velocity variations in the water column are visible. In Figure 4.6, an expanded view of the water column is shown, so that these erroneous variations are more apparent. The probable causes of these variations include bad picks, and traveltime errors caused by a non-zero-phase wavelet on the reflection series. The purpose of Figure 4.6

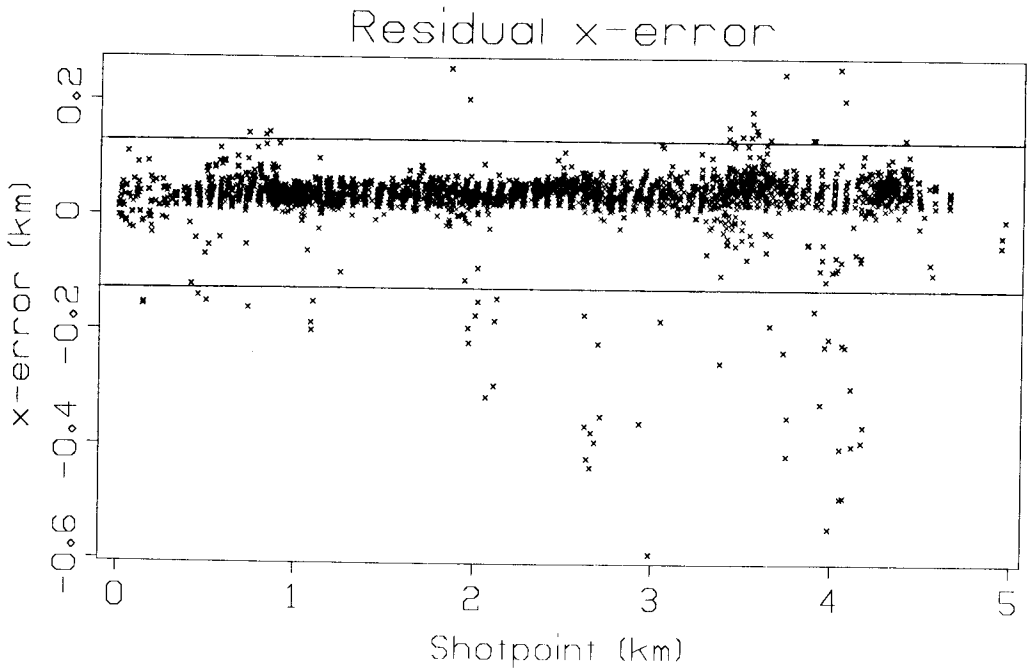

Figure 4.4: Plot of residual x_{err}. Residual x_{err} is plotted as a function of migrated midpoint location. The picked parameters outside the solid lines are filtered out; they are likely to be noise.

is to provide an idea of the possible magnitude of velocity-analysis errors. These errors are especially large in the water column because the velocity is not constrained by any intermediate reflectors between the water bottom and the surface.

Figure 4.7 shows the same depth-migrated data as Figure 4.3, plotted in a more conventional form. Figure 4.8 shows, for comparison, the picked data after time migration at the CDR velocity v_{CDR} (see section 2.3.3). There are significant differences between the two figures: for instance, the strong reflector at midpoint 1.0 km and depth 1.2 seconds in Figure 4.8 exhibits a slight anticline after depth migration.

I tracked a single horizon (the one at depth 0.95 km and midpoint 1.0 km) from midpoint 0.0 km to midpoint 2.5 km (I denote midpoints according to their distance in kilometers from the origin; the position of this origin is consistent on all plots). I used Paul Fowler's pre-stack constant-velocity migration program (Fowler, 1984) to produce a migration velocity analysis along this horizon. Figure 4.9 shows the results of the velocity analysis. Overlaid on this figure is a line representing, at the same traveltime as the analyzed horizon, the vertical-ray rms velocity. The rms velocities are determined from the interval velocities in Figure 4.1,

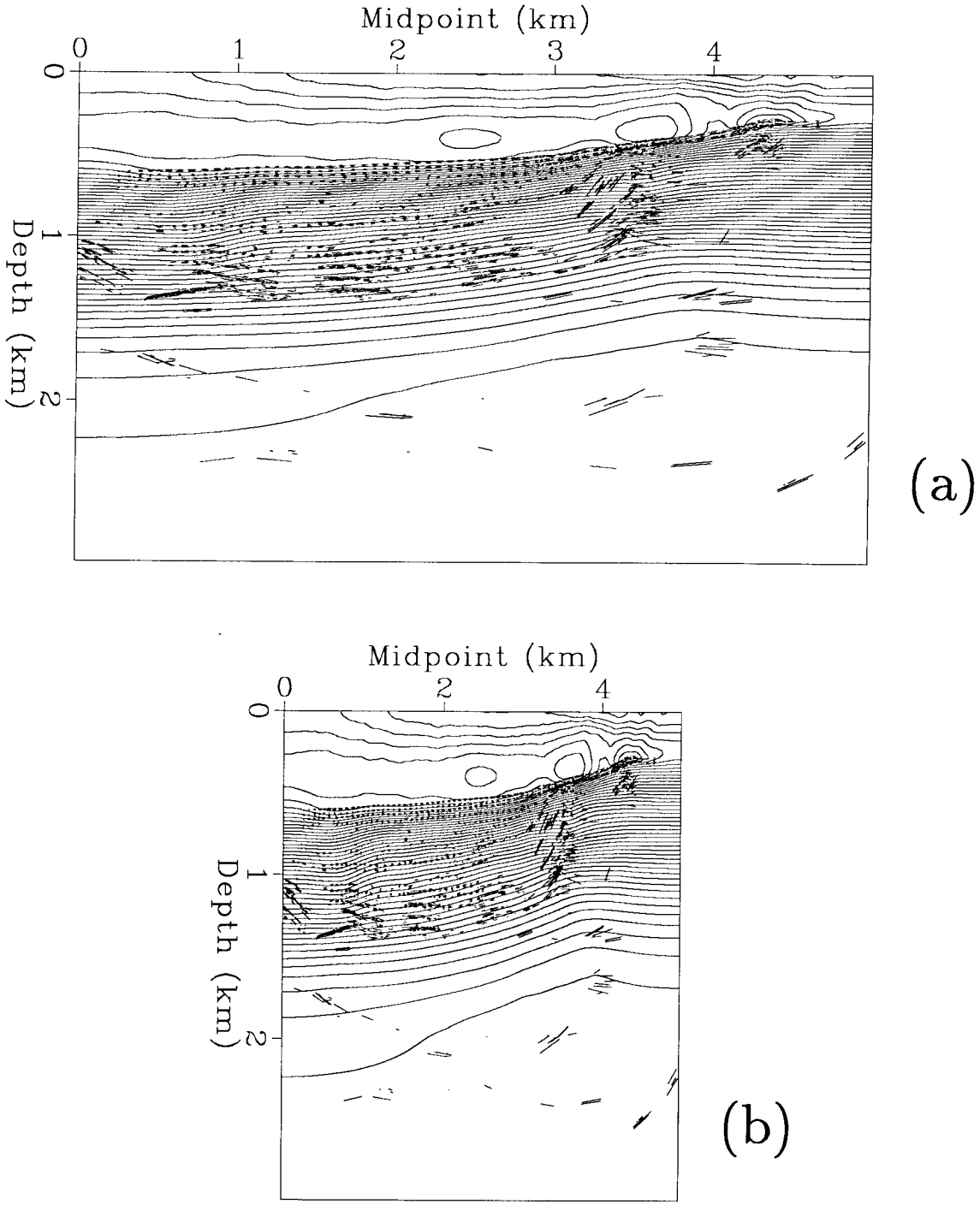

Figure 4.5: Superimposed velocity contours and migrated dip bars. The dip bars in Figure 4.3 have been superimposed on a contour plot of the velocity model. The contour interval is .025 km/sec. Panel (a) has no vertical exaggeration, while panel (b) has a 2-to-1 vertical exaggeration. Note the variations in the water column; they can be used to obtain an error estimate for the velocity inversion.

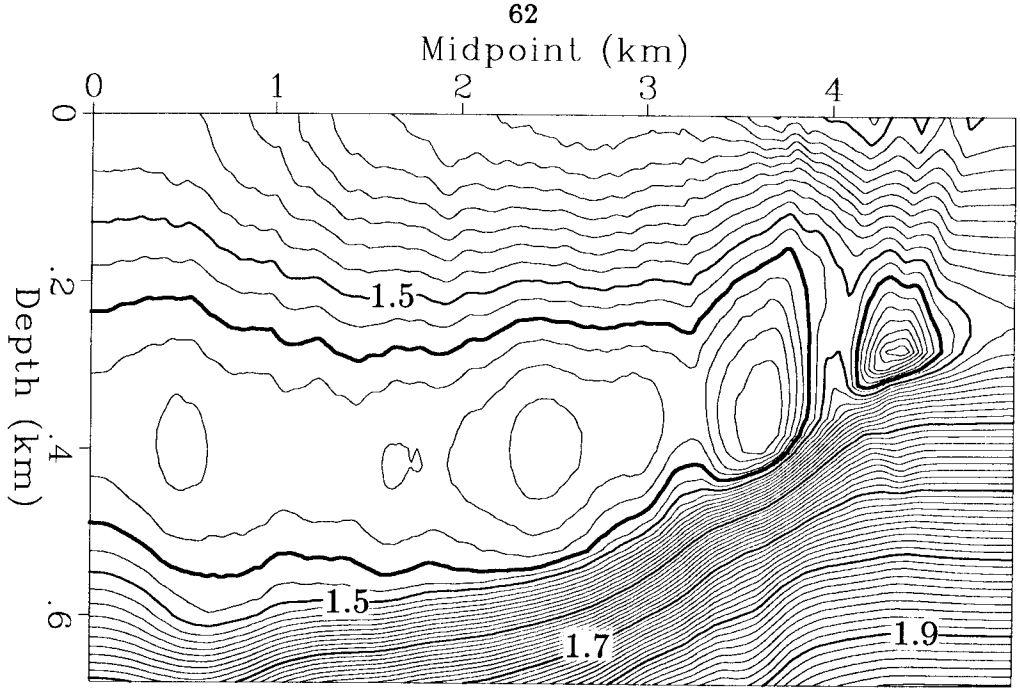

Figure 4.6: An expanded view of the water column. The contour interval in this plot is .01 km/sec. The velocity in the water column is known to be 1.48 km/sec (the thickest contour); any deviation from this velocity represents an error in the inversion procedure. The main causes of these errors are noisy data and a non-zero-phase wavelet. Notice that the lowest velocities are located just above the water bottom.

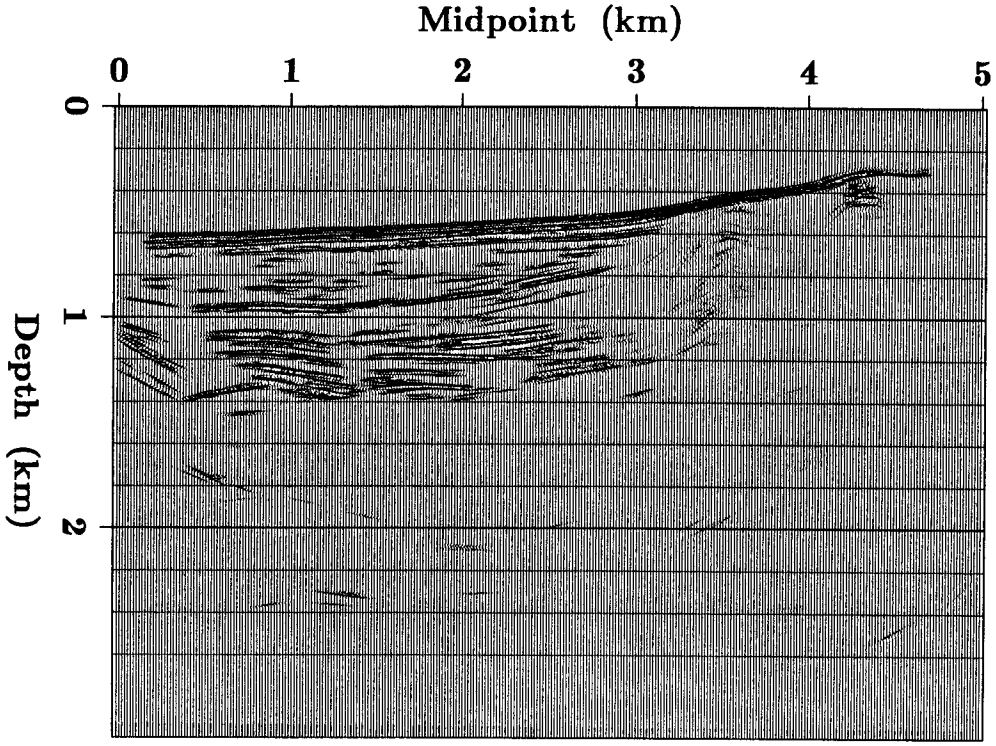

Figure 4.7: Depth-migrated data (conventional plot). This is the same migrated data as in Figure 4.3, but plotted in a more conventional form.

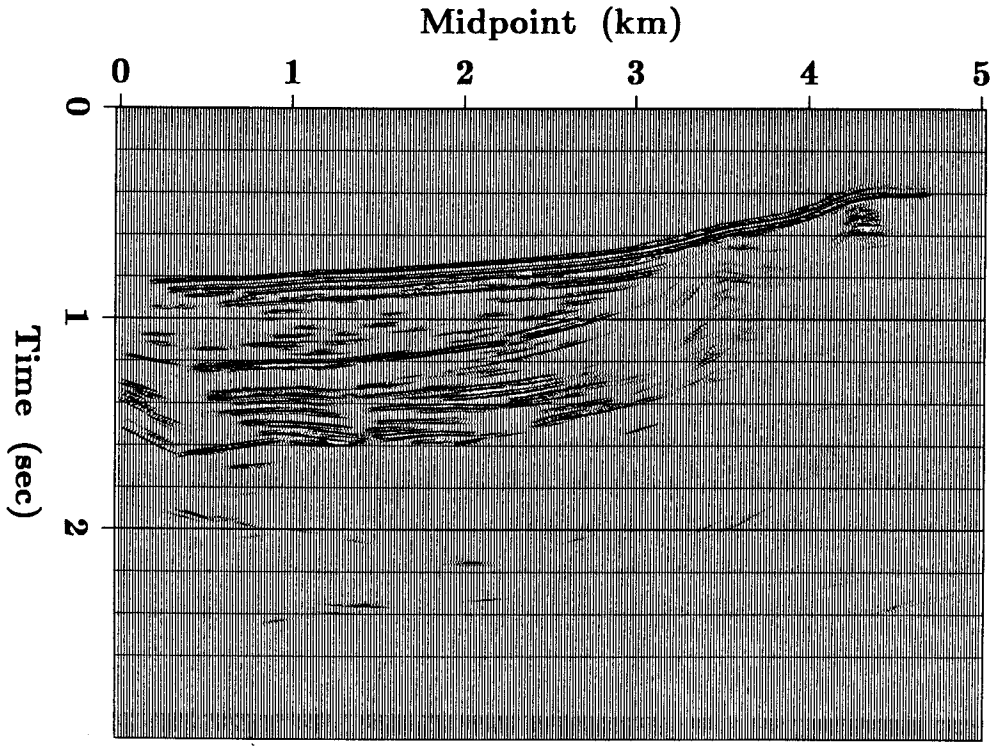

Figure 4.8: Time-migrated data ($v = v_{\mathrm{CDR}}$). The same data as in Figure 4.7 are migrated according to CDR velocities rather than computed interval velocities.

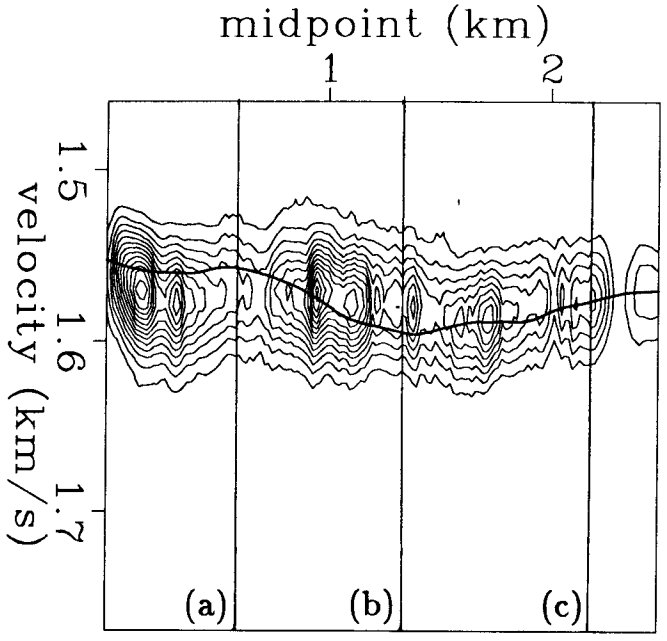

Figure 4.9: Velocity analysis along a horizon. The contour lines show a conventional rms-migration-velocity analysis along a particular horizon. The heavier line shows the corresponding rms velocity derived from Figure 4.1. The vertical lines represent the location of cross-sections (Figure 4.10).

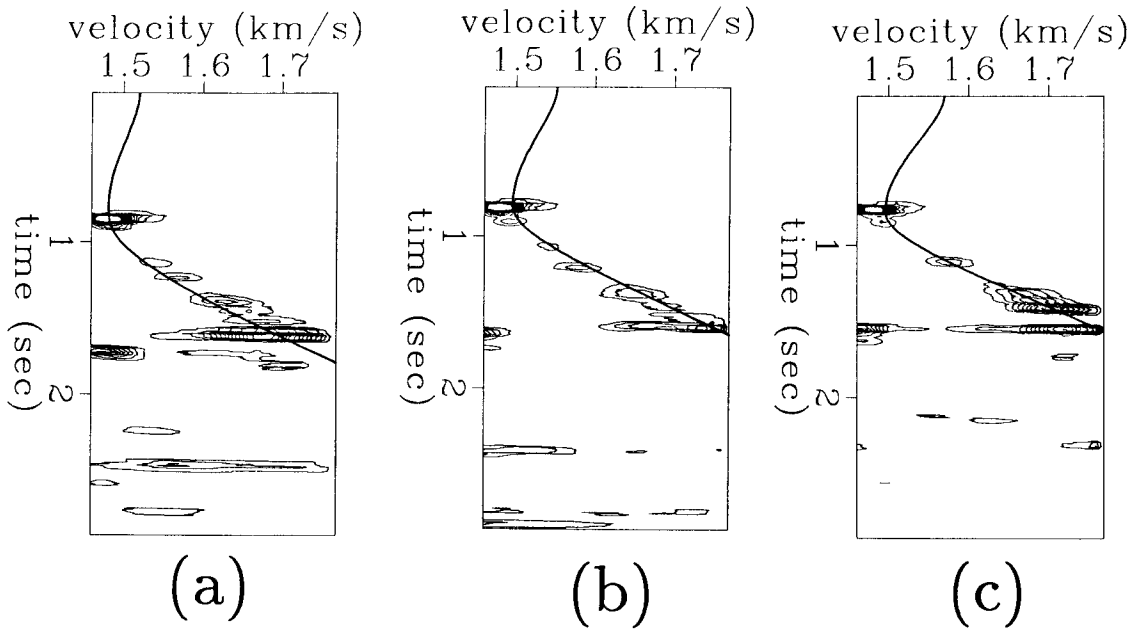

Figure 4.10: Three rms velocity analyses. The three panels are from the three midpoints designated in Figure 4.9. The contour lines show the results of a conventional migration-velocity analysis, while the heavier lines show the equivalent rms velocities derived from Figure 4.1. Notice the water-bottom multiples with a traveltime of 1.6 seconds and a velocity of 1.5 km/sec.

The vertical lines in Figure 4.9 denote midpoints where supplementary velocity comparisons were made; these comparisons are shown in Figure 4.10. Each panel in this figure shows rms migration velocity versus depth at a single midpoint. Overlaid on each panel is the vertical-ray rms velocity determined from the interval velocities in Figure 4.1.

Neither Figure 4.9 nor 4.10 shows a perfect correspondence between the interval velocity model and the migration velocity analysis. The discrepancy is not entirely surprising, since the migration velocity analysis is based on the assumption of constant velocity. An obvious problem, however, is the failure in Figure 4.10 to find the maximum of the water-bottom-reflection peaks. This discrepancy may be explained by the fact that in the tomographic velocity analysis there was no weighting by amplitude. Thus, one strong reflector is less important in the inversion than many weak reflectors. However, in conventional velocity analysis (represented by the contour lines), reflection amplitudes are used, and one strong reflection can overwhelm the weaker reflections. The tomographic velocity analysis and the conventional velocity analysis may, as a result, be focusing on different events, creating a discrepancy.